Applied Catalysis B: Environmental 179 (2015) 395–406

Contents lists available at ScienceDirect

Applied Catalysis B: Environmental

journal homepage: www.elsevier.com/locate/apcatb

Promotion effect of ultraviolet light on NO + CO reaction over Pt/TiO_2 and Pt/CeO_2–TiO_2 catalysts

Kun Huang, Liuliu Lin, Kai Yang, Wenxin Dai*, Xun Chen, Xianzhi Fu

Research Institute of Photocatalysis, State Key Laboratory of Photocatalysis on Energy and Environment, Fuzhou University, Fuzhou 350002, PR China

ARTICLE INFO

Article history:
Received 1 April 2015
Received in revised form 19 May 2015
Accepted 22 May 2015
Available online 23 May 2015

Keywords:
Nitrogen monoxide reduction
Carbon monoxide oxidation
Platinum nanoparticles
Electron transfer
Photo-assisted effect

ABSTRACT

Pt catalysts supported on TiO_2 and CeO_2–TiO_2 (Pt/TiO_2 and Pt/CeO_2–TiO_2) were prepared by a two-step precipitation–deposition method, respectively. As compared to Pt/TiO_2, Pt/CeO_2–TiO_2 exhibits a higher thermo-catalytic activity and stability for CO + NO reaction, and also exhibits a stronger effect of ultraviolet light (UV) on promoting this reaction. The in-situ FTIR results indicate that the doped CeO_2 can significantly improve the adsorption of NO at Pt/CeO_2–TiO_2, while UV light further enhance the adsorption of NO and its activation. Based on the results of Raman spectrum, electron paramagnetic resonance and the X-ray photoelectron spectroscopy testing, it is proposed that UV irradiation can cause the increase in surface electron density of Pt nanoparticles by the photo-induced electron transfer from TiO_2 to Pt. Moreover, the doped CeO_2 can further improve the electron transfer from TiO_2 to Pt through a process of $Ce^{4+} \rightarrow Ce^{3+}$ under UV irradiation, resulting in the adsorption and activation of CO and NO species at Pt/CeO_2–TiO_2. This result also indicates that the photo-excitation of supports can strengthen the strong interaction between support and metal nanoparticles, and then promote the thermo-catalytic reactivity of catalysts.

1. Introduction

As a component of automobile exhaust of great importance, nitrogen oxide is the hardest to eliminate, and the CO reduction of NO is one of the three crucial model reactions (three-way conversion reactions, TWC reactions) of automobile exhaust [1]. During the past few decades, the noble metal catalyst (especially the Pt catalyst) supported on metal oxides, as a kind of catalyst with an excellent catalytic reactivity of CO + NO reaction, has gained the most attraction on the TWC reactions [2–4]. Owing to own the excellence capacity of release/storage oxygen and the strong interaction with metal sites, the reducible oxide CeO_2 has also been introduced into the noble metal TWC catalysts [5] . Many CeO_2 doped metal oxide supports such as $CuO/CeO_2/\gamma$–Al_2O_3 [6], Cu/CeO_2 [7], $WO_3/CeO_2/ZrO_2$ [8], CeO_2/BaO–Al_2O_3 [9], NiO/CeO_2 [10] and CeO_2–ZrO_2 [11] were reported to improve the activity of both oxidizing CO and reducing NO by enhancing the dispersion of noble metals on the supports and the thermal stability of catalysts. As another reducible oxide, TiO_2 can also improve the catalytic performances of the supported noble metal catalysts for the denitration reaction. The TiO_2 doped metal oxides, such as Al_2O_3–TiO_2 [12], TiO_2–SiO_2 [13] , TiO_2–SnO_2 [14] and TiO_2–ZrO_2 [15] have been employed in the NO_x storage-reduction (NSR) and the selective catalytic reduction (SCR) reactions.

Considering that the respective advantage of TiO_2 and CeO_2, the coupled TiO_2–CeO_2 has also been employed for the TWC catalysts. TiO_2–CeO_2 exhibits a catalytic activity for selective reduction of NO with NH_3 at low temperature [16], while the TiO_2–CeO_2 supported Pd catalyst exhibits a high activity of oxidizing CO [17] and the TiO_2–CeO_2 supported Pt catalyst shows a good performance for NO + CO reaction [18] . For the process of CO + NO reaction over Pt/TiO_2–CeO_2, Bahy [18] also suggested that the strong interaction between CeO_2 and TiO_2 can cause the increase in the oxygen vacancies and the surface active sites, which facilitates the adsorption of CO and its activation at Pt sites and then the formation of the NCO intermediate species.

Zhang et al. [19] also reported that the transition metal modified TiO_2-based catalyst can cause the reduction of NO by CO under UV irradiation. They suggested that the photo-excitation of the highly dispersed Ti–O active species will play a key role during the reaction process. This proposed single-site photocatalyst theory shows that the electron transfer from O to Ti induced by UV light could enhance the adsorption of CO and NO at the transition metal (M^{n+}) sites

* Corresponding author. Tel.: +86 591 8377908; fax: +86 591 83779083.
E-mail address: daiwenxin@fzu.edu.cn (W. Dai).

http://dx.doi.org/10.1016/j.apcatb.2015.05.044
0926-3373/

highly dispersed on the single Ti–O sites, which further improve the proceeding of CO + NO reaction [20].

The above study showed that the reaction of CO + NO is mainly dependent on the adsorptions and activations of CO and NO at catalyst surface no matter during the thermo-catalytic process or during the photo-catalytic process. Our previous works [21,22] have reported that introducing UV light into the thermo-catalytic reaction system of CO oxidation over Au/TiO_2 or $Pt/CoB/TiO_2$ catalysts can promote the adsorption of CO and its activation. We also suggested that the photo-generated electrons from TiO_2 induced by UV irradiation can transfer to Au or Pt sites to increase the surface electron density of Au or Pt, resulting in the adsorption of CO and its activation at Au or Pt sites. This means that there exists a photo-thermal catalytic coupling effect on CO oxidation over the TiO_2 supported Au or Pt catalyst.

Therefore, in this present work, we have further introduced UV light into the thermo-catalytic process of CO + NO reaction over $Pt/CeO_2–TiO_2$. It is expected that UV irradiation can also promote the adsorption of CO or NO and its activation at catalyst surface, and then the reduction of NO by CO. As a comparative study, the pure TiO_2 supported Pt catalyst (Pt/TiO_2) was also tested for this reaction system. We hoped that the photo- thermal catalytic coupling effect can occur on the reaction process of CO + NO over the TiO_2 supported Pt catalyst. The result demonstrated that UV irradiation actually promoted the catalytic activities of $Pt/CeO_2–TiO_2$ and Pt/TiO_2 for CO + NO reaction. After Raman, ESR, and the X-ray photoelectron spectroscopy testing, a possible reaction mechanism for the photo-enhanced NO reduction by CO over the $Pt/CeO_2–TiO_2$ was proposed as well.

2. Experimental

2.1. Catalyst preparation

TiO_2 support [23,24] was prepared by a hydrothermal method. A 6 mL tetrabutyl titanate (TBT) was dissolved in 150 mL diethlene glycol (DEG). After stirring for 5 h, 300 mL acetone and 8.1 mL deionized water were added into the mixture. After precipitation, the suspension was filtered, washed with ethanol for several times, and dispersed in 60 mL of deionized water. And then the resulting slurry (TiO_2 precursor) was transferred into a 100 mL Teflon-lined autoclave and placed in an oven for hydrothermal treatment at 180 °C for 10 h. After the hydrothermal treatment, the produced solid precipitates were separated from the residual solution by centrifugation and washed with distilled water several times, and finally dried at 70 °C for 12 h.

For the preparation of $CeO_2–TiO_2$, a calculated amount of $CeCl_3.7H_2O$ and urea were mixed with the above TiO_2 precursor (weight ratio of CeO_2 and TiO_2 is 1/10), and were dispersed in 60 mL of deionized water. After the same hydrothermal treatment and dry process, a $CeO_2–TiO_2$ support was obtained.

$Pt/CeO_2–TiO_2$ catalyst was prepared by a precipitation–deposition method. 2.8 mL H_2PtCl_6 (0.1 g mL $^{-1}$) and 1.0 g $CeO_2–TiO_2$ support was poured into a beaker, and the pH value was adjusted to 9.0–10.0 by NaOH (0.1 mol L^{-1}). After placed for 2 h at room temperature, a 10 mL of 0.1 mol L^{-1} $NaBH_4$ aqueous solution (mixed with 0.1 mol L^{-1} NaOH) was added into the beaker. After another 2 h's stirring, the obtained solid precipitates was filtered and rinsed with the deionized H_2O several times until the remained Na^+ and Cl^- ions were removed. Finally, the powder was dried at 80 °C for 2 h, and a 1.0 wt% $Pt/CeO_2–TiO_2$ catalyst (the loading amount of Pt is about 1.0 wt%) was obtained. Similarly, a 1.0 wt% Pt/TiO_2 catalyst was also prepared by the above process with the TiO_2 support instead of $CeO_2–TiO_2$ support. In addition, keeping the content of CeO_2 at 10.0 wt%, a series of $Pt/CeO_2–TiO_2$ samples with 0.25, 0.5, 1.0, and 1.5 wt% Pt were prepared. Correspondingly, keeping the content of Pt at 1.0 wt%, a series of $Pt/CeO_2–TiO_2$ samples with 5.0, 10.0, 15.0, and 20.0 wt% CeO_2 were also prepared. In this paper, the $Pt/CeO_2–TiO_2$ samples denote the sample with a 1.0 wt% Pt content and 10.0 wt% CeO_2 content, except that the designated samples.

2.2. Characterization of catalysts

XRD patterns were obtained on a Bruker D8 advance powder X-ray diffractometer using Cu Kα radiation (λ = 0.15418 nm) operated at 40 kV and 40 mA. The textual data of the samples were measured by N_2 adsorption at liquid N_2 temperature with a micromeritics ASAP 2020 BET analyzer. The morphologies and the structures of the catalysts were characterized by an Su8000 (Hitachi) scanning electron microscope (SEM) and transmission electron microscopy (TEM) investigation together with an electron-diffraction image (JEOLJEM-2010EX with field emission gun at 200 kV). The X-ray photoelectron spectroscopy (XPS analysis) was conducted by using the Al–K X-ray beam (1486.6 eV) operated at 25 kW. All the bonding energies were calibrated to the C1s peak at 284.6 eV of the surface adventitious carbon. Photo induced electron paramagnetic resonance (EPR) signals were recorded with a Bruker A300 spectrometer both in the dark and under liquid N_2 temperature (−196 °C). The UV–vis DRS spectra were recorded at room temperature by means of a UV–vis spectrophotometer (Cary 5000). Raman spectra were carried out on LabRAM HR UV-NIR microscope (HoRIBA Jobin Yvon) employing a 532 nm excition of Ar^+ ion laser.

2.3. Catalytic performances

The evaluation of CO + NO reaction was operated in a fixed-bed flow reactor under an atmospheric pressure. In the typical reaction, the catalyst (500 mg) with a grain size of 0.2–0.3 mm was packed in a flat-plate quartz cell (30 × 20 × 0.5 mm), and heated by an electric resistance board. The temperature of the catalyst bed was monitored by a *K*-type thermocouple inserted into the reactor. During the photo-thermal reaction process, UV light (produced by a 300 W xenon lamp with a UV-reflectance filter, 300 nm < λ < 420 nm) was irradiated from the top surface of the quartz cell. For the thermal reactions (without light), the quartz cell was enclosed by Al foils to rule out light irradiations. The feed stream (composition: 0.5 vol% NO, 0.5 vol% CO, and the balance gas He) was fed at a total flow rate of 100 mL min^{-1}. Before the reactions, the catalyst was first pretreated in He atmosphere at 120 °C for 1 h. Then, the reactions were performed at a series of temperatures (60, 80, 100, 120, 150, 180, and 200 °C). After reacting for 1 h at each temperature in the dark, UV light was introduced into the reactor for 1 h. The effluent stream was analyzed by an online chemiluminescence NO_x-analyser. The NO conversion, CO conversion and N_2 selectivity were calculated as follow, respectively:

$$\text{NO conversion} = (NO_{in} - NO_{out})/NO_{in}$$

$$\text{CO conversion} = (CO_{in} - CO_{out})/CO_{in}$$

$$\text{N2 selectivity} = 2N_{2out}/NO_{in}$$

2.4. CO adsorption measurement by FT-IR

A Nicolet Nexus 670 FT-IR instrument which contains a controlled environment chamber equipped with two CaF_2 windows was employed to record the in situ FT-IR spectra, running in a range of 400–4000 cm^{-1}. An intact and thin self supporting sample pullet (15 mg) of catalyst was mounted on a holder in the chamber.

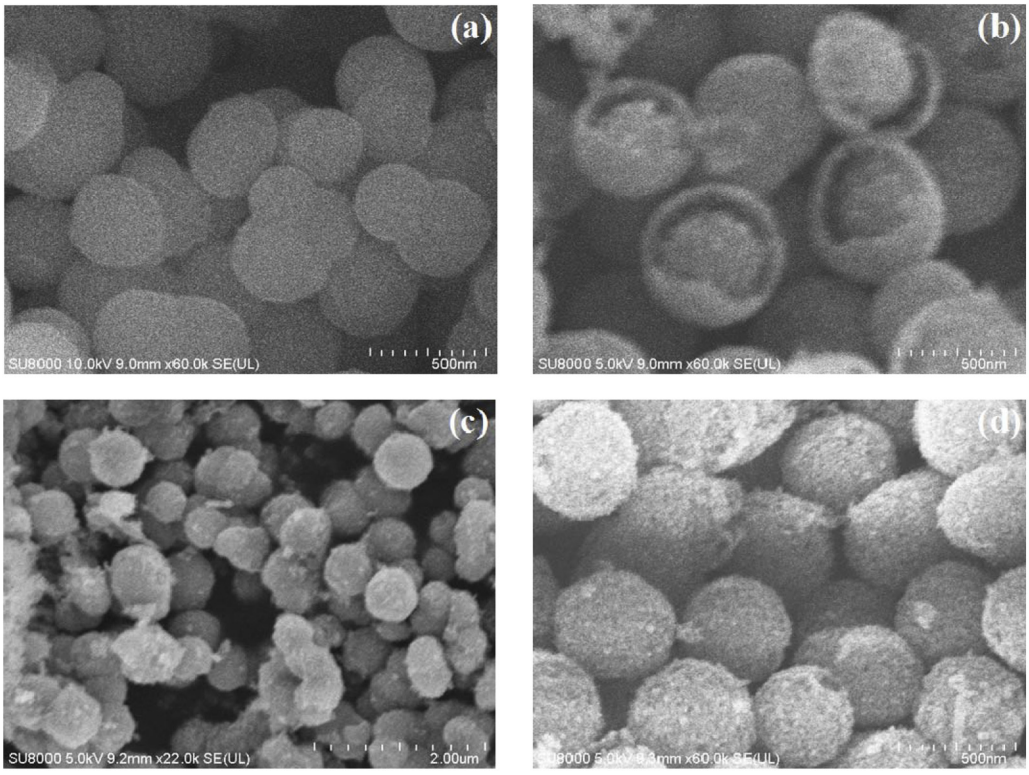

Fig. 1. SEM images of TiO_2 (a), CeO_2–TiO_2 (b), Pt/TiO_2 (c) and Pt/ CeO_2–TiO_2 (d) samples.

Before the experiment, this sample was pretreated in a vacuum at 200 °C for 2 h under a pressure of 10^{-1} Pa. After cooling to room temperature, the absorbed gas (CO and NO) was introduced into the sample. All the spectra were recorded by a DTGS KBr detector in the absorbance mode.

3. Results and discussion

3.1. Catalyst characterization

Fig. 1 shows the SEM images of different samples. The TiO_2 sample exhibits a complete solid spherical in shape with a rather narrow size distribution of about 0.4–0.6 mm (Fig. 1a). The doping CeO_2 still keeps the microsphere in exterior shape, but presents a triple-shelled hollow structure with sphere-in-sphere in the inside of microsphere (Fig. 1b). However, the loading of Pt can make the microsphere of TiO_2 or CeO_2/TiO_2 rougher on the surface (Fig. 1c and d). The HRTEM images in Fig. 2a and b show that the Pt nanoparticles with sizes of 5–8 nm are dispersed on the surface of TiO_2 or CeO_2–TiO_2 support. Moreover, the lattice fringe with d-spacing of 0.231 nm is indexed to the {1 1 1} lattice plane of Pt, while the lattice fringes with d-spacing of 0.355 nm and 0.315 nm are indexed to the {1 0 1} lattice plane of anatase and fluorite-type CeO_2, respectively (Fig. 2a and b).

The XRD patterns of TiO_2, CeO_2–TiO_2, Pt–TiO_2 and Pt–CeO_2–TiO_2 in Fig. 3 show that TiO_2 presents the structure of standard anatase (reflection peak at 2θ of 25.65°, 38.21°, 48.39°, 54.36°, 55.36°, and 63.06°). However, the characteristic diffraction peaks of CeO_2 or Pt species are not observed in the XRD pattern of CeO_2–TiO_2, Pt–TiO_2 or Pt–CeO_2–TiO_2. This indicates that the CeO_2

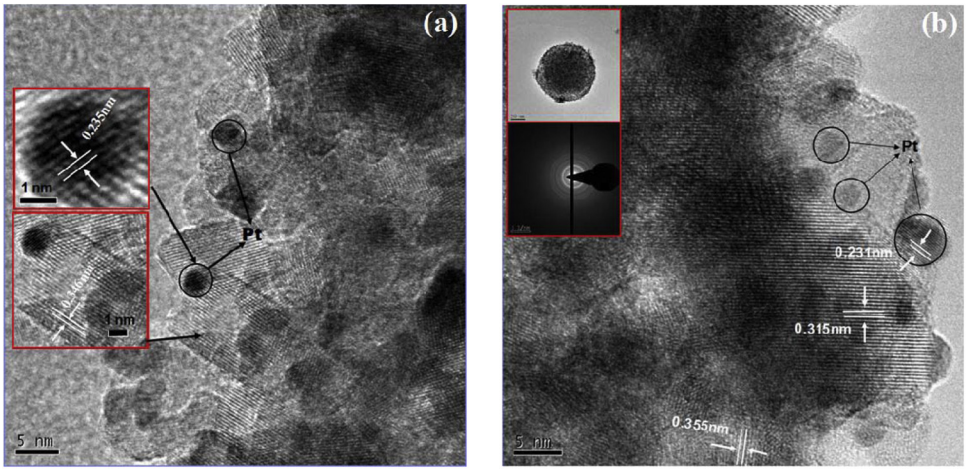

Fig. 2. HRTEM images of Pt/TiO_2 (a) and Pt/CeO_2–TiO_2 (b) samples.

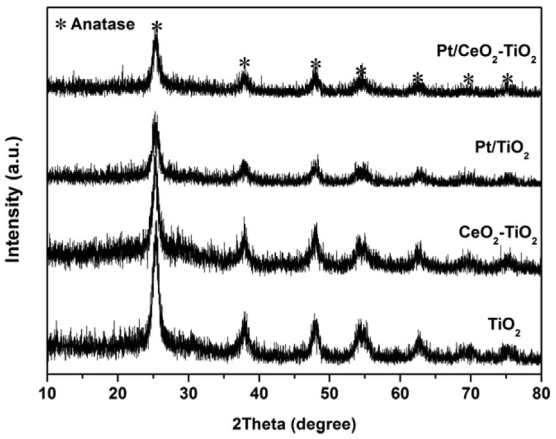

Fig. 3. XRD patterns of TiO_2, CeO_2, Pt/TiO_2 and Pt/CeO_2–TiO_2 samples.

and Pt nanoparticles are highly dispersed at the surface of TiO_2. In addition, the mean crystallite size of TiO_2 calculated by Scherrer formula is about 14 nm, while loading platinum and doping CeO_2 can cause the slight decrease in the crystallite size (seen in Table 1).

Moreover, both doping CeO_2 and loading Pt do not cause the significant change in texture properties, especially in the specific area and the pore size (seen in Fig. S1 in Supporting information (SI) and Table 1). However, the doped CeO_2 into TiO_2 can cause an increase in pore volume due to the formation of core–shell structure.

Fig. 4 shows the UV–vis diffused reflectance spectra of different samples. It is observed that all samples show a sharp absorption edge at wavelength shorter than 380 nm (attributed to the characteristic absorption of TiO_2 anatase). However, the absorption edge of CeO_2–TiO_2 exhibits a red shift (up to about 450 nm) as compared with the bare TiO_2, indicating that doping CeO_2 into TiO_2 will broaden the light absorption region. Moreover, the loading of Pt will further enhance the light absorption in visible light region. Noted that the special gaps at 350 nm are not the characteristic peaks of samples, which can be attributed to the change of light intensity induced by switching tungsten lamp to deuterium lamp at 350 nm during the testing process. The band gaps of these samples are summarized in Table 1.

3.2. Catalytic performances

Fig. 5 shows the performances of Pt/TiO_2 and Pt/CeO_2–TiO_2 for CO + NO reaction at different temperature under UV irradiation or not. As can be seen, the CO conversion, NO conversion and N_2 selectivity at each temperature ($40\,^{\circ}C < T < 200\,^{\circ}C$) over Pt/CeO_2–TiO_2

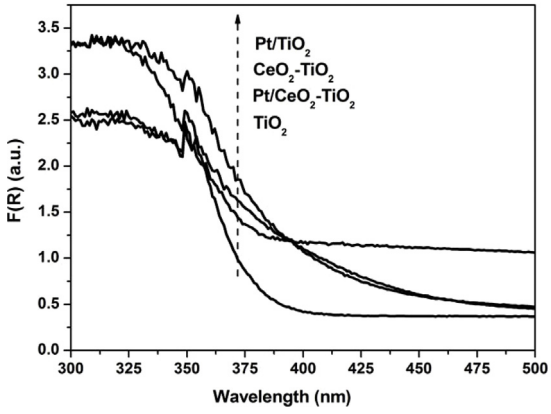

Fig. 4. UV–vis diffuse reflection spectra of TiO_2, CeO_2, Pt/TiO_2 and Pt/CeO_2–TiO_2 samples.

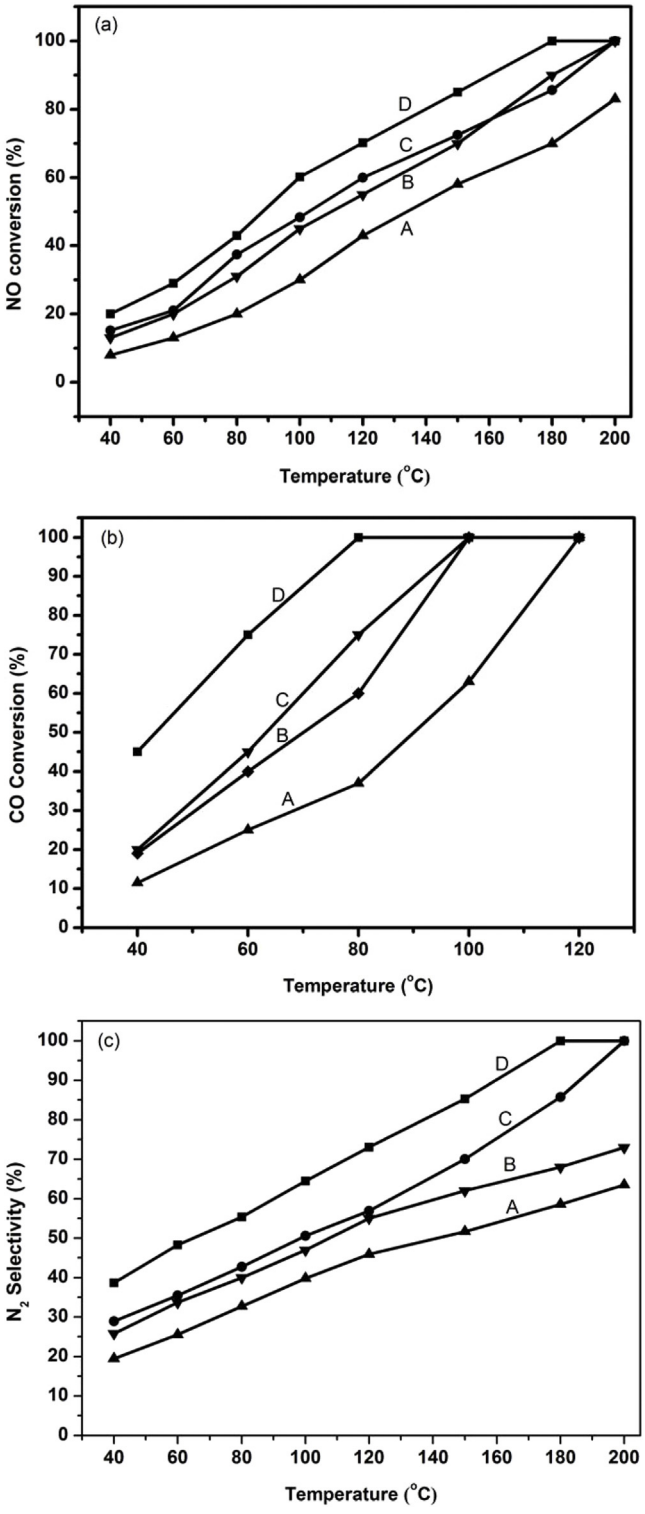

Fig. 5. NO conversion (a), CO conversion (b) and N_2 selectivity (c) at different reaction temperatures over Pt/TiO_2 and Pt/CeO_2–TiO_2 under UV irradiation or in dark: (A) Pt/TiO_2 in dark; (B) Pt/CeO_2–TiO_2 in dark; (C) Pt/TiO_2 under UV irradiation; (D) Pt/CeO_2–TiO_2 under UV irradiation.

are higher than those over Pt/TiO_2 respectively, indicating that the addition of CeO_2 into Pt/TiO_2 can promote the reduction of NO into N_2 by CO.

With the introduction of UV light, all the CO conversion, NO conversion and N_2 selectivity at each temperature increase over Pt/TiO_2 and Pt/CeO_2–TiO_2, indicating that UV irradiation could

Table 1
Texture properties of TiO_2, CeO_2–TiO_2, Pt/TiO_2 and Pt/CeO_2–TiO_2 samples.

Samples	Surface area($m^2\ g^{-1}$)	Pore volume ($ml\ g^{-1}$)	Pore diameter (nm)	Particle size(nm)	Band gap(eV)
TiO_2	172.11	0.3063	10.59	14	3.26
CeO_2–TiO_2	147.36	0.3971	9.54	11.2	2.70
Pt/TiO_2	122.32	0.3371	10.1	11.1	3.23
Pt/CeO_2–TiO_2	150.96	0.4243	9.07	12.3	2.66

promote the catalytic activities of both Pt/TiO_2 and Pt/CeO_2–TiO_2 for NO + CO reaction. Moreover, two catalysts almost exhibit the same promoted effect of UV light on this reaction.

To investigate the influences of Pt or CeO_2 content on the catalytic activity of Pt/CeO_2–TiO_2, we also compared the catalytic performances of Pt/CeO_2–TiO_2 samples with different Pt or CeO_2 contents for NO + CO reaction under UV irradiation or in dark at 10 °C, respectively (seen in SI 3). It is found that the catalytic activity of sample increases with the increase at Pt or CeO_2 content. As the Pt or CeO_2 content reaches at 1.0 wt% or 10.0 wt%, the Pt/CeO_2–TiO_2 samples already exhibit a higher catalytic activity overall (seen in Figs. S3 and S4). Based on this result, we think that the Pt/CeO_2–TiO_2 sample with a 1.0 wt% Pt and 10.0 wt% CeO_2 can fully exhibit the promoting effect of UV light on NO + CO reaction. Therefore, this Pt/CeO_2–TiO_2 sample was further applied to the following experiments.

The stability of the promoted effect of UV light on NO + CO reaction over Pt/TiO_2 and Pt/CeO_2–TiO_2 were investigated at the reaction temperature of 150 °C for an interval of 48 h in light and dark. As seen in Fig. 6a, the CO conversions over both Pt/TiO_2 and Pt/CeO_2–TiO_2 decrease in dark with the increase in reaction time. After introducing UV light into reaction system, the CO conversions over two catalysts increase and are more stable. However, the CO conversion still gradually drops down over Pt/TiO_2 but keeps stable over Pt/CeO_2–TiO_2 under UV irradiation with the increase in reaction time. Note that the NO conversions over both catalysts almost keep stable under UV irradiation or not (seen in Fig. 6b). The decrease in CO conversion as well as the stability of NO conversion means the decrease of N_2 selectivity ($2CO + 2NO \rightarrow 2CO_2 + N_2$). Here, more NO may be reduced to N_2O ($CO + 2NO \rightarrow CO_2 + N_2O$). This above result indicates that Pt/CeO_2–TiO_2 exhibits a higher catalytic activity of reducing NO to N_2 by CO than Pt/TiO_2 under UV irradiation or not. Moreover, the promoted effect of UV light on this reaction over Pt/CeO_2–TiO_2 is more stable than that over Pt/TiO_2. This advantage of Pt/CeO_2–TiO_2 may be attributed to the change in the chemical state of Pt and TiO_2 induced by CeO_2.

Fig. 7 shows the Raman spectrum of Pt/TiO_2 and Pt/CeO_2–TiO_2 samples before and after reaction. All samples present the peaks at 146, 195, 397, 515, 640 cm^{-1}, corresponding to the six Raman vibration mode of 3 Eg, 2B1 g, and A1 g. Here, the bands at 143, 195, and 393 cm^{-1} can be predominantly attributed to the O—Ti—O bending vibration and the bands 515 and 640 cm^{-1} to Ti—O stretching vibration of TiO_2 anatase [25]. As compared to that of Pt/TiO_2, the O—Ti—O bending vibration peak of Pt/CeO_2–TiO_2 make a shift to a lower wavenumber and become narrower (seen the amplified part in Fig. 7), indicating that the loading of CeO_2 can weaken the strength of O—Ti—O bending vibration. This may be attributed to the increase at the oxygen vacancies of TiO_2 induced by the doping of CeO_2. However, no peak at 462 cm^{-1} assigned to CeO_2 [26] is observed.

For the two reacted samples in dark, the peak at 149 cm^{-1} becomes stronger and makes a blue shift as compared to the two fresh samples (143 cm^{-1}), respectively. Moreover, the shift value of Pt/CeO_2–TiO_2 is greater than that of Pt/CeO_2–TiO_2 (seen the amplified part in Fig. 7). This may be attributed to the decrease at oxygen vacancies of TiO_2 (i.e., lower surface electron density of Ti sites) during reaction in dark, while the addition of CeO_2 could further decrease the oxygen vacancies of TiO_2 by the electron transfer from TiO_2 to CeO_2. For the two reacted samples under UV irradiation, the peak at 149 cm^{-1} becomes stronger but makes a red shift compared to the two reacted samples in dark, respectively (seen the amplified part in Fig. 7). This indicates that UV irradiation can also decrease the oxygen vacancies of TiO_2 due to the photo-excitation of TiO_2 (also regarded as a photo-oxidation behavior), but increase the surface electron density of TiO_2 to some extent. Moreover, the existence of CeO_2 can further decrease the oxygen vacancies by the photo-generated electron from TiO_2 to CeO_2 ($Ti^{3+} + CeO_2 \rightarrow Ti^{4+} + Ce_2O_3$). This means that the reducibility of CeO_2 ($CeO_2 + e \rightarrow Ce_2O_3$) maybe cause the change at intensity of O—Ti—O binding.

In order to further verify the reducibility of CeO_2 ($Ce^{4+} + e \rightarrow Ce^{3+}$) over Pt/CeO_2–TiO_2 under UV irradiation, the EPR experiments of Pt/CeO_2–TiO_2 samples after reacting at

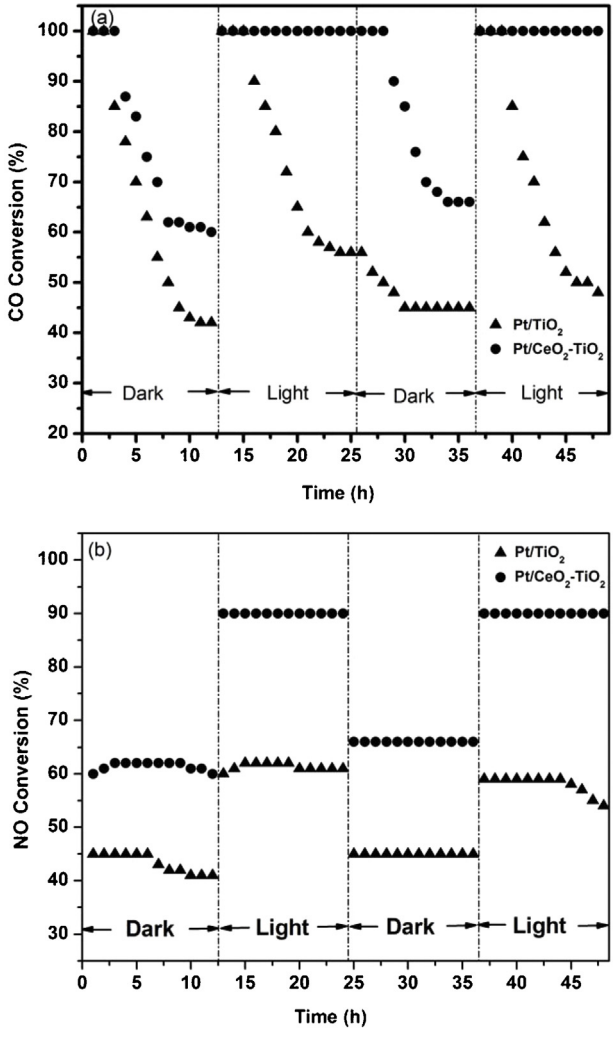

Fig. 6. Conversions of CO (a) and NO (b) as function of reaction time at 150 °C over Pt/TiO_2 and Pt/CeO_2–TiO_2 under UV irradiation or in dark, respectively.

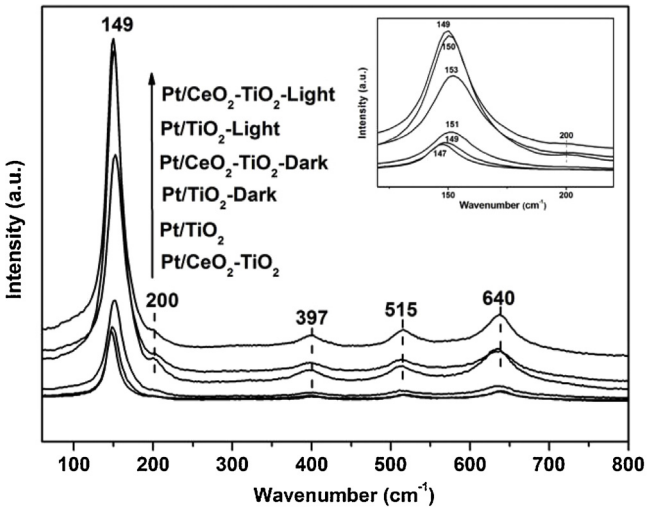

Fig. 7. Raman spectra of Pt/TiO_2 and Pt/CeO_2–TiO_2 samples before and after reactions in dark or under UV irradiation.

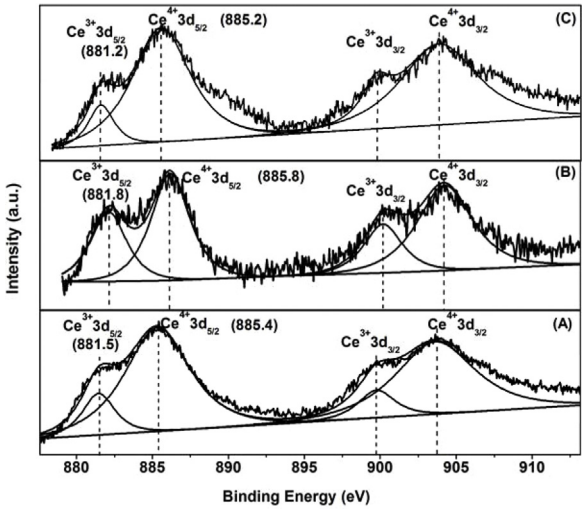

Fig. 9. High-resolution XPS spectra of Ce3d of Pt/CeO_2–TiO_2 sample under different treatment: (A) the fresh sample; (B) reacted in dark; and (C) reacted under UV irradiation.

different temperatures under UV irradiation or not were conducted, respectively. As seen in Fig. 8, the peak at $g = 1.997$, assigned to the captured electrons released from oxygen vacancies in TiO_2 (Ti^{3+}) [27], appears in all samples. Compared to the sample reacted at 100 °C in dark, a new peak at $g = 1.991$, assigned to the Ce^{3+} [28], can be observed over the sample at 150 °C in dark (Fig. 8B), indicating that Ce species mainly exhibits in the state of Ce^{4+} at 100 °C but in the states of both Ce^{4+} and Ce^{3+} at 150 °C. Meanwhile, the peak at $g = 2.004$, corresponding to the O^{2-} species, can be observed over the sample at 150 °C but not at 100 °C. This result shows that CeO_2 is not active enough to release O^{2-} radicals at a lower temperature but can do at a higher temperature. This process can be explained that CeO_2 accept the heat-excited electrons from TiO_2 to release O^{2-} ($2CeO_2 + 2e$ (heat-excited) $\rightarrow Ce_2O_3 + O^{2-}$). With the introduction of UV light, the peak at $g = 1.991$ is observed over the sample reacted at 100 °C (seen in Fig. 8B and D), indicating that UV light can cause the formation of Ce^{3+} at 100 °C. Moreover, the observed peak at $g = 2.004$ at 100 °C also means that UV irradiation can lead to the formation of O^{2-} species (seen in Fig. 8B and D). Here, CeO_2 can accept the photo-generated electrons from TiO_2 to release the O^{2-} radicals ($2CeO_2 + 2e_{cb}$ (photo-excited) $\rightarrow Ce_2O_3 + O^{2-}$). Without a doubt, this behavior induced by the photo-excitation of TiO_2 can also occur at 150 °C (UV irradiation causes the increase at two peaks at $g = 1.991$ and $g = 2.004$, seen in Fig. 8D). Noted that the captured heat-excitated electrons ($g = 1.997$) can be identified from the photo-excited electrons ($g = 1.996$) from TiO_2.

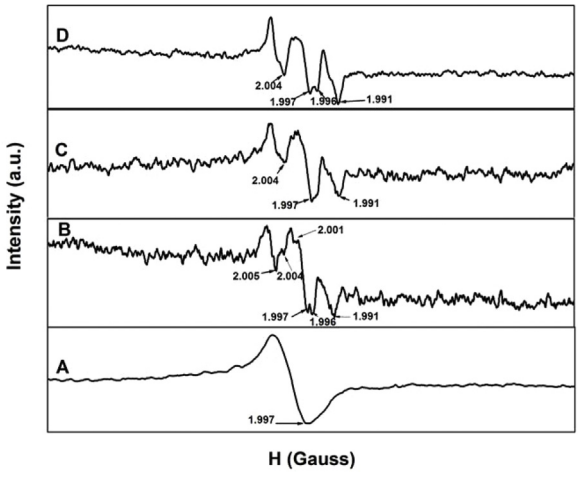

Fig. 8. EPR spectrum of the reacted Pt/CeO_2–TiO_2 samples under UV irradiation or not: (A) at 100 °C in dark; (B) at 100 °C under UV irradiation; (C) at 150 °C in dark; (D) at 150 °C under UV irradiation.

The above result shows that the electron transfer behavior between TiO_2 and CeO_2 can be caused by heat or UV light. However, the heat-excitated electron transfer only occurs at a higher temperature, while the photo-excitated electron transfer can occur at a lower temperature. This may be one reason that UV light can promote the catalytic activity of Pt/CeO_2–TiO_2 at a lower temperature.

In fact, CeO_2 is a good support with a fine structure for paramagnetic transition metal ions like Ti^{4+} [29]. Introduction of CeO_2 into TiO_2 will be in favor of the availability of electrons produced by heat or UV irradiation [30]. For Pt/CeO_2–TiO_2 sample in this work, heating or UV irradiation will lead to the activation of CeO_2, resulting in the formation of oxygen deficient non-stoichiometric cerium oxide as well as the O^{2-} species. This process may be somewhat responsible for the higher activation of NO and CO reaction compared to Pt/TiO_2.

In our previous works [31], we suggested that a higher surface electron density of Pt and Au would be favorable for the activation of CO species adsorbed at Pt or Au surface, and then promote the oxidation of CO. For the reaction of NO + CO over Pt/CeO_2–TiO_2 under UV irradiation, it may be also the increase in Pt surface electron density induced by the activation of CeO_2 that promotes the adsorption and activation of NO and CO. To confirm this viewpoint, the surface electron density of Pt and the adsorption behaviors of CO and NO over Pt/CeO_2–TiO_2 under UV irradiation or not were studied via XPS and FT-IR testing, and were also compared with that over Pt/TiO_2.

Fig. 9 shows the high-resolution XPS spectra of Ce3d of Pt/CeO_2–TiO_2 sample under different treatment condition. As can be seen, Ce is mainly existed in the valence of Ce^{3+} and Ce^{4+} over all samples, corresponding to the oxygen storage/release process of $2CeO_2 \leftrightarrow Ce_2O_3 + O^{2-}$ [32] . After Pt/CeO_2–TiO_2 reacted in dark, the area ratio of $Ce^{4+}3d$ to $Ce^{3+}3d$ decreases means that CeO_x experiences the storage oxygen process overall. Here, CeO_2 will accept heat-excitated electrons from TiO_2 ($2CeO_2 + 2e$ (heat-excitated) $\rightarrow Ce_2O_3 + O^{2-}$). For the Pt/CeO_2–TiO_2 sample reacted under UV irradiation, the decreased ratio of Ce^{3+}–Ce^{4+} implies that CeO_2 experiences the release oxygen process overall. However, the

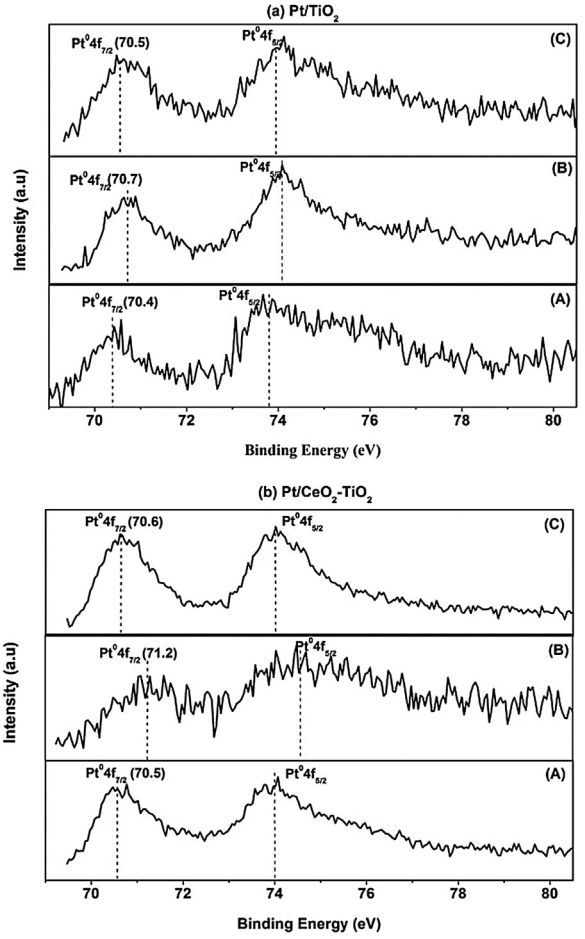

Fig. 10. High-resolution XPS spectra of Pt4f of (a) Pt/TiO_2 and (b) Pt/CeO_2–TiO_2 samples under different treatment: (A) the fresh sample; (B) reacted in dark; and (C) reacted under UV irradiation.

lower binding energy (BE) of $Ce^{3+}3d_{5/2}$ than that in dark (881.2 eV vs. 881.8 eV) means that UV irradiation can increase the electron density of Ce^{3+} sites. This result shows that CeO_2 can accept the electrons from TiO_2 and then take part in the process of storage/release oxygen over CeO_x under UV irradiation.

This electron transfer from TiO_2 to CeO_2 over Pt/CeO_2–TiO_2 under UV irradiation can be also verified by the XPS result of O1s and Ti2p of Pt/TiO_2 and Pt/CeO_2–TiO_2 samples reacted under UV irradiation or in dark (seen in Fig. S2 in SI). As compared to the Pt/TiO_2, Pt/CeO_2–TiO_2 shows the lower BE values of O1s and Ti2p after reacting in dark, but it exhibits the higher BE values of O1s and Ti2p after reacting under UV irradiation. This means that the more photo-excitated electrons transfer from TiO_2 to CeO_2 or Pt sites due to the presence of CeO_2.

The presence of CeO_2 in Pt/TiO_2 maybe also take part in the process of electron transfer between Pt and TiO_2. As seen in Fig. 10(a), Pt species mainly exhibit in the state of Pt^0 (the standard BE of $Pt^0 4f_{7/2}$ = 71.1 eV) [33] in the fresh Pt/TiO_2. After reacted in the dark, Pt species still exist mainly in the state of Pt^0, but the BE of $Pt^0 4f_{7/2}$ increases from 70.4 to 70.7 eV, indicating that the decrease at the surface electron density of Pt. However, for the Pt/TiO_2 sample reacted under UV irradiation, the BE of $Pt^0 4f_{7/2}$ is lower than that in dark (70.5 eV vs. 70.7 eV). This means that UV irradiation can maintain the surface electrons at Pt sites. As compared to the fresh Pt/TiO_2, the fresh Pt/CeO_2–TiO_2 also exists mainly in the state of Pt^0 (BE = 70.5 eV) but with a higher BE of $Pt^0 4f_{7/2}$ (70.5 eV vs. 70.4 eV) (seen in Fig. 10b). After Pt/CeO_2–TiO_2 reacted in dark, the BE of $Pt^0 4f_{7/2}$ increases from 70.5 to 71.2 eV. However, the Pt/CeO_2–TiO_2 sample reacted under UV irradiation presents a lower BE of $Pt^0 4f_{7/2}$ (70.6 eV). This indicates that CeO_2 can decrease the surface electron density of Pt during the reaction process in dark but increase that under UV irradiation. This also means that CeO_2 can act as an electron transfer intermediates to promote the photo-generated electron transfer from TiO_2 to Pt. It may be the higher electron density of Pt surface to be responsible for the stability of catalytic activity of Pt/CeO_2–TiO_2 under UV irradiation (seen in Fig. 6).

The above XPS results indicate that UV irradiation can promote the electron enrichment on Pt sites by the photo-excitation of TiO_2 over Pt/TiO_2, while the introduction of CeO_2 can further promote the electron transfer from TiO_2 to Pt sites over Pt/CeO_2–TiO_2 samples. Meanwhile, UV irradiation may facilitates the oxygen release/storage process of CeO_2. The two common effects will promote the adsorption and activation of NO or CO at Pt/CeO_2–TiO_2, and then promote the oxidation of CO and reduction of NO.

In our previous study [34], we have found that a high electron density at Au or Pt surface can be favorable for the adsorption and activation of CO, and then its oxidation. Therefore, the in-situ FT-IR testing for adsorbing NO, CO and CO + NO over Pt/TiO_2 and Pt/CeO_2–TiO_2 were also performed, respectively.

Fig. 11a and b show the FT-IR spectra of Pt/TiO_2 and Pt/CeO_2–TiO_2 adsorbing CO under UV irradiation or in dark. As seen in Fig. 11a, for Pt/TiO_2 adsorbing CO in dark (curve A), the peak at 1645 cm^{-1} (assigned to the H_2O chemisorbed at the TiO_2 sites) and three peaks at 1443, 1413, and 1343 cm^{-1} (assigned to the different carboxylate-like species) are observed [35,36], which can be can be ascribed to the result of the adsorbed CO at TiO_2 sites reacting with the adjacent lattice oxygen of TiO_2 [35]. Under UV irradiation (curve B in Fig. 11a), the increased peak at 1645 cm^{-1} and the decreased peaks at 1443 and 1413 cm^{-1} mean that UV light can promote the carboxylate-like species at TiO_2 sites to react with the surface hydroxyls over Pt/TiO_2 (resulting in the formation of H_2O [35]). For Pt/CeO_2–TiO_2 adsorbing CO in dark (curve C in Fig. 11), two observed broad peaks at 1500 and 1414 cm^{-1} can be assigned to the carboxylate-like species at CeO_2 or TiO_2 sites [37]. Moreover, the two peak areas greatly increase with the introduction of UV light (curve D in Fig. 11a), indicating that UV irradiation can promote the adsorption of CO at CeO_2 or TiO_2 sites over Pt/CeO_2–TiO_2.

More importantly, UV irradiation can also cause the change of CO adsorption at Pt sites for Pt/TiO_2 and Pt/CeO_2–TiO_2 samples. For Pt/TiO_2 in dark (curve A in Fig. 11b), two observed peaks at 2079 and 2346 cm^{-1} can be attributed to the linearly adsorbed Pt^0–CO and CO_2 [38] , respectively. With the introduction of UV light (curve B in Fig. 11b), the increased peak of Pt^0–CO shifts to a low wavenumber (from 2079 to 2076 cm^{-1}), and is further split into a new absorption peak at about 2050 cm^{-1} which may be attributed to the Pt–CO–Pt [18]. Moreover, the intensity of CO_2 at peak of 2346 cm^{-1} is significantly increased, indicating that UV irradiation promote the oxidation of CO at Pt sites even in the absence of O_2. For Pt/CeO_2–TiO_2 in dark (curve C in Fig. 11b), besides the peaks at 2082 and 2346 cm^{-1} (assigned to the linearly adsorbed Pt^0–CO and CO_2, respectively), a new peak at about 2193 cm^{-1} (corresponding to the adsorbed β–Ti^{4+}–CO) appears [39–41] compared to that of Pt/TiO_2. This indicates that the presence of CeO_2 is favorable for the adsorption and activation of CO at TiO_2 sites. Under UV irradiation (curve D in Fig. 11b), the peak of Pt^0–CO shifts to a lower wavenumber (from 2082 to 2078 cm^{-1}), and the increased peak of β- Ti^{4+}–CO also shifts to a lower wavenumber (from 2193 to 2172 cm^{-1}) along with a split peak at 2208 cm^{-1} (assigned to the α-Ti^{4+}–CO) [42]. Similarly to that of Pt/TiO_2, UV irradiation also promotes the formation of CO_2 over Pt/CeO_2–TiO_2. These results show that UV irradiation can promote the adsorption and activation of CO at Pt sites over both Pt/TiO_2 and Pt/CeO_2–TiO_2, consistent with

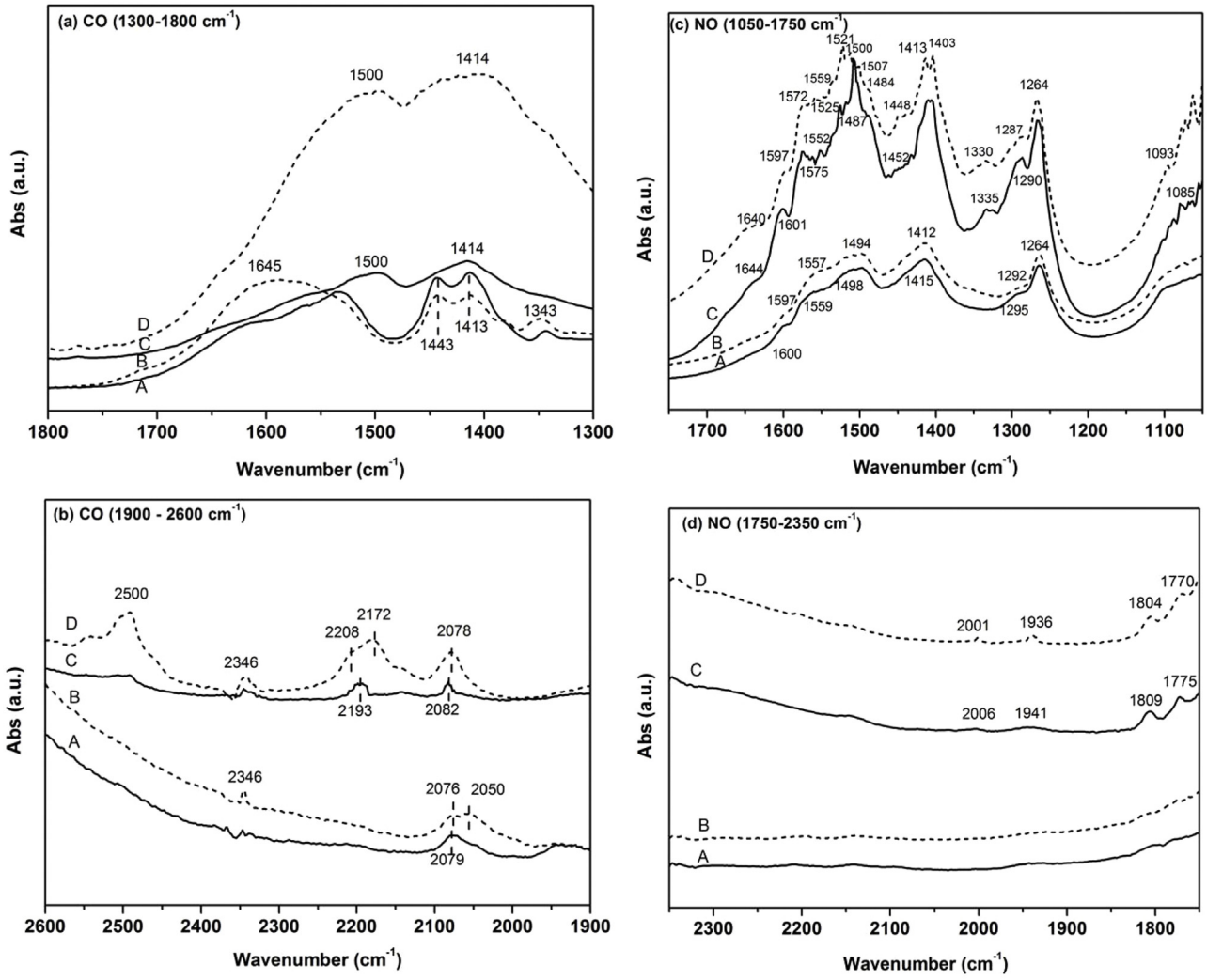

Fig. 11. FT-IR spectra of adsorbing CO (a and b) and NO (c and d) over samples under UV irradiation or not, respectively: (A) Pt/TiO_2 in dark; (B) Pt/TiO_2 under UV irradiation; (C) Pt/CeO_2–TiO_2 in dark; (D) Pt/CeO_2–TiO_2 under UV irradiation.

the result of $Pt/Co–B/TiO_2$ in our previous work [34] . Here, the obtained electrons at Pt surface from TiO_2 can transfer to the π^* orbital of CO molecule adsorbed at Pt sites according by the principle of d–π^* back-donation [43], resulting in a weaker C—O bond (i.e., the infrared vibrational spectrum of CO adsorbed at Pt sites shifts to a lower frequency).

As compared to that of Pt/TiO_2, another new broad peak at about 2500 cm^{-1}, induced by the isolated O^{2-} species interact with the surface hydroxyl group at support [44], appears after Pt/CeO_2–TiO_2 adsorbing CO in dark (curve C) and becomes remarkably strong under UV irradiation (curve D). This also indirectly indicates that the introduction of CeO_2 really leads to the formation of O^{2-} species which can be further generated by UV light. Note that the bridged adsorption peak of CO at Pt sites (Pt–CO–Pt, corresponding to the peak at 2050 cm^{-1}), induced by the agglomeration of Pt nanoparticles [18], does not appear over Pt/CeO_2–TiO_2 under UV irradiation. This indicates that UV irradiation can keep the isolated dispersion of Pt nanoparticles at TiO_2 surface induced by CeO_2 over Pt/CeO_2–TiO_2, but promote the agglomeration of Pt nanoparticles at TiO_2 surface over Pt/TiO_2. This may be one reason that Pt/TiO_2 shows a low stability of catalytic activity for CO + NO reaction even under UV irradiation (seen in Fig. 6).

Fig. 11c and d show the FT-IR spectra of Pt/TiO_2 and Pt/CeO_2–TiO_2 adsorbing NO under UV irradiation or in dark. For Pt/TiO_2 adsorbing NO in dark (curve A), the observed peaks at 1600, 1559, 1498, 1415, and 1295 cm^{-1} can be attributed to the different types of nitrate and nitrite adsorbed at different sites or in different geometry. There into, the peaks at 1498 and 1295 cm^{-1} are assigned to the monodentate NO_3^-, the peak at 1600 cm^{-1} to the bridged NO_3^-, and the peak at 1415 cm^{-1} to the Ti^{4+}–ONO^- [45] . Moreover, no new peak can be observed over Pt/TiO_2 with the introduction of UV light except that the peaks shift red somewhat (curve B in Fig. 11c). For the Pt/CeO_2–TiO_2 sample after adsorbing NO in dark (curve C in Fig. 11c), in addition to the peaks at 1601, 1552, 1520, 1410, 1290 cm^{-1}, the new peaks at 1644, 1575, 1525, 1487, 1452, 1335, and 1085 cm^{-1}, assigned to the nitrate and nitrite [46], are also observed. There into, the peaks at 1525, 1487 cm^{-1} can be attributed to the monodentate NO_3^-, the peak at 1575 cm^{-1} to the bridged NO_3^-, the peak at 1452 cm^{-1} to the Ce^{4+}–NO_2, and the two peaks at 1335 and 1085 cm^{-1} to the Ce^{4+}–$N_2O_2^{2-}$ (*cis*) and the hyponitrite ion $N_2O_2^{2-}$ (*trans*), respectively [47]. In addition, the peaks at 1941 and 2002 cm^{-1} assigned to the (NO_x^-)–Ti^{4+}–NO, the peak at 1809 cm^{-1} assigned to the Pt^{2+}–NO, and the peak at 1775 cm^{-1} assigned to the Pt^0–NO [48] can be also observed in the region of 1750–2350 cm^{-1} (curve C in Fig. 11d). As compared to the result of Pt/TiO_2 adsorbing NO, it is found that the existence of CeO_2 promotes the of NO adsorption at Pt and Ti^{4+} sites, and the formation of Ce^{4+}–NO_2, nitrate and nitrite species. Similarly to that

of Pt/TiO_2, no new peak appears on Pt/CeO_2–TiO_2 under UV irradiation (curve D in Fig. 11c). However, the peaks corresponding to the Ce^{4+}–NO_2, Ce^{4+}–$N_2O_2^{2-}$ (*cis*) and hyponitrite ion $N_2O_2^{2-}$ (*trans*) shift to a higher wavenumber (from 1452, 1335, and 1085 cm^{-1} to 1460, 1339, and 1093 cm^{-1}, respectively, seen in curves C and D in Fig. 11c) under UV irradiation, while the peaks corresponding to the (NO_x^-)–Ti^{4+}–NO, Pt^{2+}–NO and Pt^0–NO shift to a lower wavenumber (from 2006, 1941, 1809, and 1775 cm^{-1} to 2001, 1936, 1804, and 1770 cm^{-1}, respectively, seen in curves C and D in Fig. 11d). This means that UV irradiation can strengthen the respective vibration of the adsorbed NO-contained species at CeO_x sites, but weaken those (i.e., activating N—O bond) at TiO_2 and Pt sites. This indicates that UV irradiation can lead to the decrease at surface electron density of CeO_x sites but to the increase at that of TiO_2 and Pt sites.

This above result shows that doping CeO_x into Pt/TiO_2 can decompose NO and promote NO activation at Pt and Ti^{4+} sites. Moreover, the introduction of UV light can promote the electron transfer among TiO_2, CeO_2 and Pt, resulting in the increase at the surface electron density of Pt sites and then the adsorption and activation of NO at Pt sites.

To further describe the behavior of UV light on the reaction of NO + CO over Pt/TiO_2 and Pt/CeO_2–TiO_2, the in-situ FT-IR spectra of two samples co-adsorbing NO and CO were recorded. As shown in Fig. 12, Pt/TiO_2 exhibits several absorption peaks in the region of 1000–1850 cm^{-1} (curve A in Fig. 12a), corresponding to the different species adsorbed at TiO_2 sites, such as bridge NO_3^- (1600 cm^{-1}), acetate (1575 cm^{-1}), monodentate NO_3^- (1504 and 1294 cm^{-1}), and carbonate species (1448, 1412, and 1321 cm^{-1}). Also, the peak at 1412 cm^{-1} can be partly attributed to the Ti^{4+}–ONO^- species [45]. In addition, the peaks at 2346 and 2087 cm^{-1} assigned to the CO-induced species including the physisorbed CO_2 and Pt^0–CO species [38] are observed in the region of 1800–2600 cm^{-1} (curve A in Fig. 12b). As compared to the case of Pt/TiO_2 adsorbing single CO or NO in dark (seen in Fig. 11), the new species of CO_2 (2346 cm^{-1}) means that CO maybe interact with NO to form CO_2 over Pt/TiO_2 in dark. After introducing UV light into Pt/TiO_2 (curve B in Fig. 12a), the peaks in the region of 1000–1850 cm^{-1} seem to become smaller, but a new peak at 1658 cm^{-1} (assigned to the symmetrical N_2O_3) appears [49]. This indicates that UV irradiation can promote the adsorbed intermediate species to further interact and form new species over Pt/TiO_2. Noted that the peaks of monodentate NO_3^- and monodentate carbonate make a shift to some extent (from 1504 and 1321 cm^{-1} to 1481 and 1336 cm^{-1}, respectively), which can be attributed to the change at surrounding environment of the species induced by reaction.

Moreover, UV light can make the peak of Pt^0–CO shift to a lower wavenumber (from 2087 to 2077 cm^{-1}) with a increased intensity, and lead to the formation of Pt–NCO and Pt^{2+}–CO species (corresponding to the peaks at 2200 and 2138 cm^{-1}, respectively) [18]. This indicates that UV light can be conducive to the adsorption and activation of CO and NO at Pt and TiO_2 sites, consistent with the result of adsorbing single CO or NO in Fig. 11. Note that another new peak at 2296 cm^{-1} (assigned to Ti^{4+}–NO^- species) [45] can be observed over Pt/TiO_2 after co-adsorbing NO and CO under UV irradiation (curve B in Fig. 12b). Meanwhile, the peak at 1944 cm^{-1} (assigned to Ti^{4+}–NO) disappears with the introduction of UV light over Pt/TiO_2, indicating that Ti^{4+}–NO maybe accept the photo-generated electrons from TiO_2 to form Ti^{4+}–NO^- species. However, the two peaks at 2296 and 1944 cm^{-1} do not appear in the case of Pt/TiO_2 after adsorbing single NO under UV irradiation or not (seen in curve B in Fig. 11c). This indicates that the presence of CO may be beneficial to the adsorption of NO at TiO_2 sites over Pt/TiO_2, for the preferential adsorption of CO at Pt sites maybe suppresses the adsorption of NO at Pt sites.

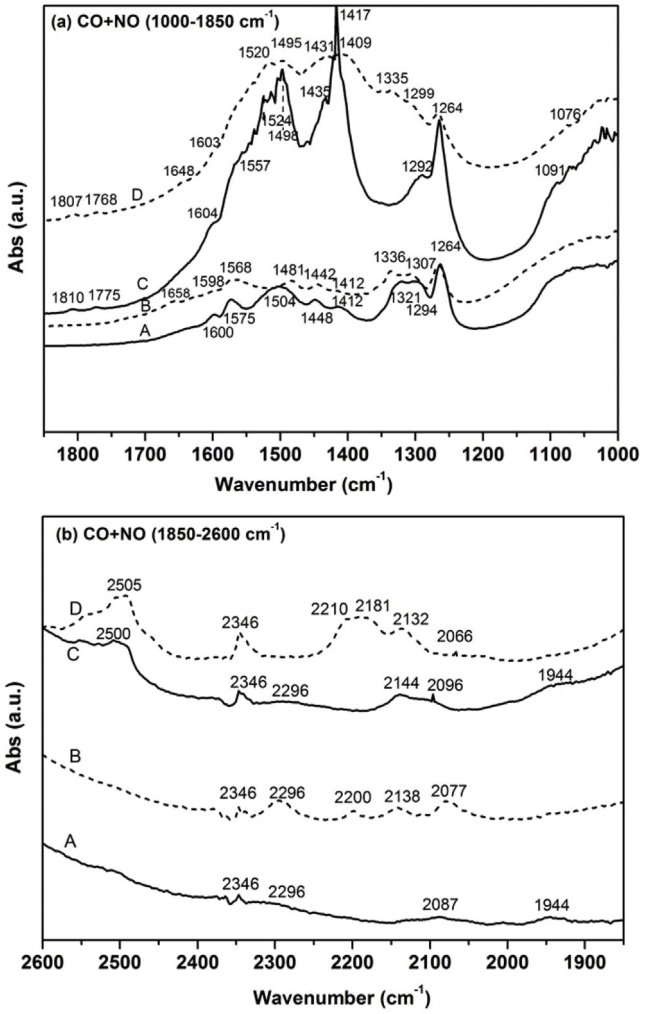

Fig. 12. FT-IR spectra of co-adsorbing CO and NO (a and b) over samples under UV irradiation or not: (A) Pt/TiO_2 in dark; (B) Pt/TiO_2 under UV irradiation; (C) Pt/CeO_2–TiO_2 in dark; (D) Pt/CeO_2–TiO_2 under UV irradiation.

For Pt/CeO_2–TiO_2 sample, co-adsorbing CO and NO in dark can also cause the formation of different species (curve C in Fig. 12a and b). As compared to the result of Pt/CeO_2–TiO_2 adsorbing single NO, the peaks at 1435 and 1336 cm^{-1} (assigned to Ce^{4+}–NO_2^- and Ce^{4+}–$N_2O_2^{2-}$, respectively) can not be observed in the region of 1000–1850 cm^{-1} (curve C in Fig. 12a) due to be overlapped by the carbonate [50]. With the introduction of UV light, the peaks of Pt^{2+}–NO, Pt^0–NO and $N_2O_2^{2-}$ at CeO_x site shift to the lower wavenumber (from 1810, 1775, and 1091 cm^{-1} to 1807, 1768, and 1075 cm^{-1}, respectively, seen in curve D in Fig. 12a), indicating that UV light promotes the activation of NO adsorbed at Pt or CeO_x sites. In the range of 1850–2600 cm^{-1}, Pt/CeO_2–TiO_2 exhibits four peaks at 2096, 2144, 2296, and 2346 cm^{-1} after co-adsorbing CO and NO in dark (curve C in Fig. 12b), corresponding to Pt^0–CO, Pt^{2+}–CO, Ti^{4+}–NO^-, and CO_2, respectively [44]. Moreover, a larger peak at the region from 1400 to 1500 cm^{-1} appears, indicating that CeO_2 will promote the formation of intermediates such as acetate, monodentate NO_3^- and monodentate carbonate species [51]. Under UV irradiation, the peaks of Pt^0–CO and Pt^{2+}–CO species shift to a lower wavenumber (from 2096 and 2144 cm^{-1} to 2066 and 2132 cm^{-1}, respectively, seen in curve D in Fig. 12b). Moreover, two new peaks at 2181 and 2210 cm^{-1} (assigned to β- type Ti^{4+}–CO and α-type Ti^{4+}–CO species) [18] appear, but the peak at 2296 cm^{-1} (attributed to the Ti^{4+}–NO^-) disappears with the introduction of UV light. However, the formed Pt–NCO species (2200 cm^{-1}) over Pt/TiO_2 after

co-adsorbing CO and NO under UV irradiation (seen in curve B in Fig. 12b) is much less than that over Pt/CeO_2–TiO_2. Since the formed NCO species (Pt–CO + NOads → Pt–NCO + Oads) is regarded as an important intermediate specie for NO reduction to N_2 [48], Pt/CeO_2–TiO_2 exhibits a higher activity and selectivity for the reaction of NO + CO than Pt/TiO_2 under UV irradiation due to the former possessing the more Pt–NCO species.

Noted that the peak at 1944 cm^{-1} (assigned to Ti^{4+}–NO) disappears with the introduction of UV light over Pt/CeO_2–TiO_2, indicating that the Ti^{4+}–NO can react rapidly with Pt–CO under UV irradiation. Moreover, the peaks at 1496 and 1417 cm^{-1} (attributed to the acetate and monodentate carbonate, respectively) remarkably weaken with the introduction of UV light (seen curve D in Fig. 12a), indicating that UV irradiation can promote the further reaction of these intermediates over Pt/CeO_2–TiO_2. Similarly, to the result of Pt/CeO_2–TiO_2 adsorbing single CO, the increased peak at about 2500 cm^{-1} under UV irradiation (curve D in Fig. 12b), induced by the isolated O^{2-} species interacting with the surface hydroxyl group at support [44], means that UV irradiation still promote the formation of O^{2-} species over Pt/CeO_2–TiO_2 even in the presence of NO.

However, it can be seen from the FT-IR spectra in Figs. 11 and 12, each curve appears the peak at about 1266 cm^{-1}. This can be attributed to the absorption characteristic peak of vacuum grease used to seal the quartz chamber during the testing process.

Based on the above FT-IR result, it can be concluded as follows: (1) UV irradiation can promote the adsorption and activation of CO at Pt sites over both Pt/TiO_2 and Pt/CeO_2–TiO_2. (2) UV irradiation can not promote the adsorption and activation of NO over Pt/TiO_2, but can promote that over Pt/CeO_2–TiO_2. (3) Doping CeO_2 into Pt/TiO_2 will lead to the formation of O^{2-} species, which can be further promoted by UV light. (4) Doping CeO_x into Pt/TiO_2 can promote the activation of NO at Pt and TiO_2 sites under UV irradiation, and also benefit to the formation of intermediate species of NO such as $N_2O_2^{2-}$, NO_2 at CeO_x sites. (5) The presence of CO maybe suppresses the adsorption of NO at Pt sites but promotes that at TiO_2 sites over both Pt/TiO_2 and Pt/CeO_2–TiO_2 due to the preferential adsorption of CO at Pt sites. (6) The promoted formation of NCO species (as an important intermediate species for NO reduction to N_2) over Pt/CeO_2–TiO_2 induced by UV light is much more than that over Pt/TiO_2. (7) The reaction of NO + CO over Pt/CeO_2–TiO_2 or Pt/TiO_2 are mainly dependent on the adsorbed CO at Pt sites and the adsorbed NO at TiO_2 or CeO_x sites.

Further based on the results of XPS, EPR, Raman testing of samples under UV irradiation or not, we suggest that the adsorption behavior of CO or NO at Pt/CeO_2–TiO_2 or Pt/TiO_2 is mainly determined to the surface electron density of Pt and Ti sites. CeO_2 can promote the electron transfer between TiO_2 and Pt by the release/storage oxygen process, while UV irradiation can further promote the electron transfer among CeO_2, TiO_2 and Pt sites by exciting TiO_2. In fact, many studies have ever reported that the presence of Ce^{3+} can make the valence electrons be in an unbalanced state, resulting in the formation of vacancies and unsaturated bonds at the surface of Pt catalyst, which is favorable to the increase in surface chemisorption oxygen for NO activation [52].

Referring to the thermo-catalytic process of NO + CO reaction over the supported Pt catalyst [48], the reaction process of CO + NO over Pt/TiO_2 or Pt/CeO_2–TiO_2 under UV irradiation can be described as follows:

I. Process of CO + NO reaction over Pt/TiO_2 under UV irradiation

(1) Generation and transfer of photo-excitation electrons

(a) Photo-excitation of TiO_2:

$$TiO_2 + h\nu \rightarrow TiO_2(e_{cb}^-, h_{vb}^+)$$

(b) Photo-generated electrons transfer from TiO_2 to Pt sites:

$$Pt + e_{cb}^- \rightarrow Pt(e)$$

(2) Adsorption processes of CO

(a) CO and NO are adsorbed at electron-rich Pt sites:

$$Pt(e) + CO \rightarrow \{Pt{-}C{=}O\}$$

(b) NO is adsorbed at Ti^{4+} sites and then reacts with lattice oxygen to form NO_3^- species [39]:

$$NO + Ti^{4+} \rightarrow Ti^{4+} - NO$$

$$Ti^{4+}{-}NO + TiO_2(O_L) \rightarrow Ti^{4+}{-}NO_3^- + Ti^{3+} + e$$

Meanwhile, the adsorbed NO at Ti^{4+} sites accepts the photo-generated electrons to form Ti^{4+}–NO^- species:

$$Ti^{4+}{-}NO + e_{cb}^- \rightarrow Ti^{4+}{-}NO^-$$

This Ti^{4+}–NO^- species is stable and difficult to be reduced.

(3) NO species reacting with CO species

(a) The formed NO_3^- species react with the activated CO adsorbed at Pt sites to form Pt–NCO and N_2O

$$Ti^{4+}{-}NO_3^- + \{Pt{-}C{=}O\} \rightarrow Pt{-}NCO + N_2O + Ti^{4+}e$$

$$2Pt{-}NCO \rightarrow N_2 + CO_2 + 2Pt$$

(b) N_2O reacting with oxygen vacancy to produce N_2.

$$N_2O + Ti^{3+}[O_v] \rightarrow N_2 + TiO_2$$

(4) The produced electrons will recombined with holes:

$$TiO_2(e) + TiO_2(h\nu b) \rightarrow TiO_2$$

During the above processes, UV light can promote the adsorption and activation of CO at Pt sites (Process (2a)), and then promote its oxidation by NO.

II. Process of CO + NO reaction over Pt/CeO_2–TiO_2 under UV irradiation

(1) Generation and transfer of photo-excitation electrons

(a) Photo-excitation of TiO_2:

$$TiO_2 + h\nu \rightarrow TiO_2(e_{cb}^-, h_{vb}^+)$$

(b) CeO_2 goes through an oxygen release/storage process by accepting the photo-generated electrons:

$$2CeO_2 + e_{cb}^- \leftrightarrow Ce_2O_3 + O_L^{2-}$$

This can be acted as a release oxygen process.

(c) Photo-generated electrons transfer from TiO_2 or CeO_2 to Pt sites:

$$Pt + e_{cb}^- \rightarrow Pt(e)$$

(2) Adsorption processes of CO and NO

(a) CO and NO are adsorbed at electron-rich Pt sites:

$$Pt(e) + CO \rightarrow \{Pt{-}C{=}O\}$$

$$Pt(e) + NO \rightarrow \{Pt{-}NO\}$$

(b) NO is adsorbed at Ce^{3+} sites in the state of $-N_2O_2^{2-}$:

$$2Ce^{3+} + 2NO \rightarrow Ce^{3+}{-}N_2O_2^{2-}$$

(c) NO is adsorbed at Ti^{4+} sites and then reacts with lattice oxygen to form NO_3^- species

$$NO + Ti^{4+} \rightarrow Ti^{4+}{-}NO^-$$

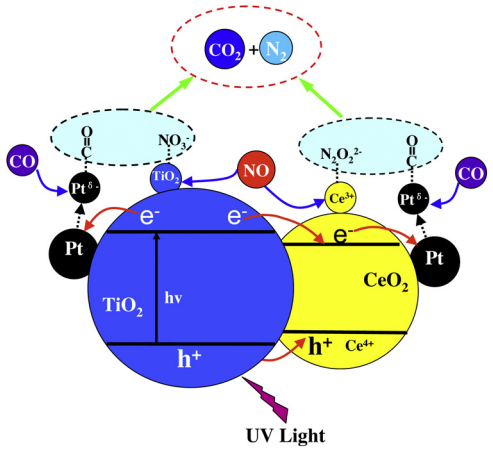

Fig. 13. Schematic of NO + CO reaction over Pt/CeO_2–TiO_2 under UV irradiation.

$$Ti^{4+}\text{–}NO + TiO_2(O_L) \rightarrow Ti^{4+}\text{–}NO_3^- + Ti^{3+} + e$$

(3) NO species reacting with CO species

(a) NO species adsorbed at Pt sites react with CO adsorbed at Pt sites to form Pt–NCO species, and then produce N_2 and CO_2:

$$\{Pt\text{–}NO\} + \{Pt\text{—}C{=}O\} \rightarrow Pt\text{–}NCO + O^{2-}$$

$$2Pt\text{–}NCO \rightarrow N_2 + CO_2 + 2Pt$$

(b) $N_2O_2^{2-}$ species formed at Ce^{3+} sites react with CO adsorbed at Pt sites to produce N_2 and CO_2:

$$Ce^{3+}\text{–}N_2O_2^{2-} + O^{2-} \rightarrow CeO_2 + N_2$$

This process also completes the storage process of CeO_x.

(c) Formed NO_3^- species react with the activated CO adsorbed at Pt sites to form Pt–NCO and N_2O, similarly to that case over Pt/TiO_2:

$$Ti^{4+}\text{–}NO_3^- + \{Pt\text{—}C{=}O\} \rightarrow Pt\text{–}NCO + N_2O + Ti^{4+} + e$$

$$2Pt\text{–}NCO \rightarrow N_2 + CO_2 + 2Pt$$

$$N_2O + Ti^{3+}[O_v] \rightarrow N_2 + TiO_2$$

As compared to the case of Pt/TiO_2, the reaction process over Pt/CeO_2–TiO_2 under UV irradiation exhibits different reaction pathway: the CO species adsorbed at Pt sites not only react with the NO species at TiO_2 sites, but also react with the NO species at Pt or CeO_x sites. Moreover, the photo-excitation of TiO_2 can lead to the electron transfer among TiO_2, CeO_2 and Pt sites and then promote the activations of both CO and NO at Pt or TiO_2 or CeO_x sites, resulting in a higher catalytic activity and selectivity of NO reducing by CO to N_2.

The above proposed mechanism of CO reaction with NO over Pt/CeO_2–TiO_2 under UV irradiation can also be described in Fig. 13. During the processes, the photo-generated electrons of TiO_2 induced by UV light can transfer to CeO_2 and then to Pt, resulting in the increase at surface electron density of Pt sites. Meanwhile, CeO_2 itself acts as an active site to take part in the reaction process. More importantly, the reducibility of CeO_2 (Ce^{4+}/Ce^{3+}, i.e., the release/storage oxygen behavior of CeO_x) will be beneficial to maintain the balance of valence states of Pt, CeO_2 and TiO_2, and then keep a higher stability of catalytic activity Pt/CeO_2–TiO_2 under UV irradiation. This study implies that the photo-generated electrons induced by the band-gap excitation of TiO_2 can act as electron donor (instead of the traditional electron additives) to promote the thermal catalytic reduction of NO by CO to N_2 over the TiO_2 supported Pt catalyst. In other words, the photo- excitation of supports can strengthen the strong interaction between support and metal nanoparticles, and then promote the thermo-catalytic reactivity of catalysts. This work maybe provide a new approach to eliminate automobile exhaust.

9. Conclusions

Pt/CeO_2–TiO_2 catalyst prepared by the hydrothermal precipitation method exhibits high catalytic activity and high selectivity N_2 for reaction of CO + NO. Introduction of UV light can remarkably promote the thermal catalytic activity and its stability of Pt/CeO_2–TiO_2 for this reaction. Based on the results of Raman spectroscopy, EPR and XPS results, it is proposed that this promotion of UV light in reduction of NO by CO to N_2 can be mainly stemmed from the photo- generated electron transfer from TiO_2 support to the adjacent Pt sites by CeO_2, resulting in the increase in surface electron density of Pt and the subsequent enhanced adsorption and activation of CO and NO molecules at Pt sites. Moreover, the release/storage oxygen behavior of CeO_x (Ce^{4+}/Ce^{3+}) can be beneficial to maintain the balance of valence states of Pt, CeO_2 and TiO_2, and then keep a higher stability of catalytic activity Pt/CeO_2–TiO_2 under UV irradiation. This study shows that the photo-excitation behavior of TiO_2 support maybe act as an electron additive to be introduced into a thermal catalytic reaction of NO + CO over the TiO_2 supported catalyst.

Acknowledgments

This work was financially supported by the National Natural Science Foundation of China (nos. 21073037 and 2127037), the National Basic Research Program of China (973 Program, no. 2014CB239303) and Science & Technology Plan Project of Fujian Province (no.2014Y2003).

Appendix A. Supplementary data

Supplementary data associated with this article can be found, in the online version, at http://dx.doi.org/10.1016/j.apcatb.2015.05.044

References

[1] S. Roy, M.S. Hegde, G. Madras, Appl. Energy. 86 (2009) 2283–2297.
[2] F. Reith, S.G. Campbell, A.S. Ball, A. Pring, G. Southam, Earth Sci. Rev. 131 (2014) 1–21.
[3] H.Y. Su, X.K. Gu, X.F. Ma, Y.H. Zhao, X.H. Bao, W.X. Li, Catal. Today 165 (2011) 89–95.
[4] A.K. Prashar, S. Mayadevi, P.R. Rajamohanan, R.N. Devi, Appl. Catal. A – Gen. 403 (2011) 91–97.
[5] J. Kašpar, P. Fornasiero, M. Graziani, Catal.Today 50 (1999) 285–298.
[6] C.Y. Ge, L.C. Liu, Z.T. Liu, X.J. Yao, Y. Cao, C.J. Tang, F. Gao, L. Dong, Catal. Commun. 51 (2014) 95–99.
[7] J.X. Yuan, L.L. Ping, C.Y. Xu, Z.X. Ming, J. Mol. Catal. A – Chem. 197 (2003) 193–205.
[8] H.O. Zhu, J.R. Kim, S.K. Ihm, Appl. Catal. B – Environ. 86 (2009) 87–92.
[9] L. Fang, X.Q. Wang, M.Q. Shen, Q.Q. Zhang, J. Wang, Chem. Eng. J. 222 (2013) 401–410.
[10] Z.C. Si, D. Weng, X.D. Wu, Z.R. Meng, R. Ran, Catal. Today 201 (2013) 122–130.
[11] X.Q. Wang, B.K. Zhai, M. Yang, W.P. Han, X. Shao, Mater. Lett. 112 (2013) 90–93.
[12] B.M. Reddy, K.N. Rao, G.K. Reddy, P. Bharali, J. Mol. Catal. A – Chem. 253 (2006) 44–51.
[13] M.S. Marth, K.L. Walther, A. Wokaun, J. Non-Cryst. Solids 143 (1992) 93–111.
[14] K.R. Li, Y.J. Wang, S.R. Wang, B.L. Zhu, S.M. Zhang, W.P. Huang, S.H. Wu, J. Nat. Gas Chem. 18 (2009) 449–452.
[15] Y.P. Zhang, X.Q. Zhu, K. Shen, H.T. Xu, K.Q. Sun, C.C. Zhou, J. Colloid Interface Sci. 376 (2012) 233–238.
[16] R. Zhang, Q. Zhong, W. Zhao, L.M. Yu, H.X. Qu, Appl. Surf. Sci. 289 (2014) 237–244.
[17] H.Q. Zhu, Z.F. Qin, W.J. Shan, W.J. Shen, J.G. Wang, J. Catal. 233 (2005) 41–50.

[18] Z.M.E. Bahy, MRC 2 (2013) 136–147.
[19] J.L. Zhang, Y. Hu, M. Matsuoka, H. Yamashita, M. Minagawa, H. Hidaka, M. Anpo, J. Phys. Chem. B 105 (2001) 8395–8398.
[20] T. Toyao, J. Morishima, M. Saito, Y. Horiuchi, T. Kamegawa, G. Martra, S. Coluccia, M. Matsuoka, M. Anpo, J. Catal. 299 (2013) 232–239.
[21] Z.X. Ding, H.Y. Yang, J.F. Liu, W.X. Dai, X. Chen, X.X. Wang, X.Z. Fu, Appl. Catal. B – Environ. 101 (2011) 326–332.
[22] K. Yang, J.F. Liu, R.R. Si, X. Chen, W.X. Dai, X.Z. Fu, J. Catal. 317 (2014) 229–239.
[23] W.G. Yang, F.R. Wan, Q.W. Chen, J.J. Li, D.S. Xu, J. Mater. Chem. 20 (2010) 2870–2876.
[24] J. Qi, K. Zhao, G.D. Li, Y. Gao, H.J. Zhao, R.B. Yu, Z.Y. Tang, Nanoscale 6 (2014) 4072–4077.
[25] M. Lubas, J.J. Jasinski, M. Sitarz, Spectrochim. Acta. A 133 (2014) 867–871.
[26] Y. Guhel, J. Bernard, B. Boudart, Microelectron. Eng. 118 (2014) 29–34.
[27] K. Yang, Y.X. Li, K. Huang, X. Chen, X.Z. Fu, W.X. Dai, Int. J. Hydrogen Energy 39 (2014) 18312–18325.
[28] J. Soria, A.M. Arias, J.M. Coronado, Colloids, Surf. A: Physicochem. Eng. Asp. 115 (1996) 215–221.
[29] J. Kašpar, P. Fornasiero, M. Graziani, Catal. Today 50 (1999) 285–298.
[30] Y.Y. Ji, T.J. Toops, M. Crocker, Catal. Lett. 119 (2007) 257–264.
[31] X.H. Lin, K. Yang, R.R. Si, X. Chen, W.X. Dai, X.Z. Fu, Appl. Catal. B – Environ. 147 (2014) 585–591.
[32] A. Trovarelli, Catal. Rev. 38 (1996) 439–520.
[33] Z.J. Mei, Y. Li, M.H. Fan, Chem. Eng. J. 259 (2015) 293–302.
[34] H.R. Zheng, H.Y. Yang, R.R. Si, W.X. Dai, X. Chen, X.X. Wang, P. Liu, X.Z. Fu, Appl. Catal. B – Environ. 105 (2011) 243–247.
[35] W.X. Dai, X. Chen, X.P. Zheng, Z.X. Ding, X.X. Wang, P. Liu, X.Z. Fu, Chem. Phys. Chem. 10 (2009) 411–419.
[36] J.D. Grunwaldt, M. Maciejiewski, O.S. Becker, P. Fabrizioli, A. Baiker, J. Catal. 186 (1999) 458–469.
[37] T. Baidya, P. Bera, B.D. Mukri, S.K. Parida, O. Kröcher, M. Elsener, M.S. Hegde, J. Catal. 303 (2013) 117–129.
[38] K. Hadjiivanov, J. Lamotte, Langmuir 13 (1997) 3374–3381.
[39] N. Li, Q.Y. Chen, L.F. Luo, W.X. Huang, M.F. Luo, G.S. Hua, Ji.Q. Lu, Appl. Catal. B: Environ. 143 (2013) 523–532.
[40] C. Li, Y. Sakata, T. Arai, K. Domen, K. Maruya, T. Onishi, J. Chem. Soc. Faraday Trans. I 85 (1989) 1451–1461.
[41] J. Guzman, S. Carrettin, A. Corma, J. Am. Chem. Soc. 127 (2005) 3286–3287.
[42] K. Hadjiivanov, V. Bushev, M. Kantcheva, Langmuir 10 (1994) 464–471.
[43] G. Blyholder, J. Phys. Chem. 68 (1964) 2772–2777.
[44] S. Tanaka, M. Taniguchi, J. Nucl. Sci. Technol. 248 (1997) 101–105.
[45] M.A. Debeila, N.J. Coville, M.S. Scurrell, G.R. Hearne, Appl. Catal. A – Gen. 291 (2005) 98–115.
[46] M. Kantcheva, J. Catal. 204 (2001) 479–494.
[47] M. Niwa, Y. Furukawa, J. Colloid Interface Sci. 86 (1982) 260–265.
[48] T. Baidya, P. Bera, B.D. Mukri, J. Catal. 303 (2013) 117–129.
[49] K. Hadjiivanov, H.K. Zinger, Phys. Chem. Chem. Phys. 2 (2000) 2803–2806.
[50] Y. Wang, A. Zhu, Y.Z. Zhang, C.T. A, X.F. Yanga, C. Shi, Appl. Catal. B – Environ. 81 (2008) 141–149.
[51] Z. Say, E.I. Vovk, V. Bukhtiyarov, E. Ozensoy, Appl. Catal. B – Environ. 143 (2013) 89–100.
[52] M. Casapu, J.D. Grunwaldt, M. Maciejewski, F. Krumeich, Appl. Catal. B – Environ. 78 (2008) 288–300.